

GraphBGS: Background Subtraction via Recovery of Graph Signals

Jhony H. Giraldo, Thierry Bouwmans
 Laboratoire MIA, La Rochelle Universit, France
 {jgiral01, tbouwman}@univ-lr.fr

Abstract

Graph-based algorithms have been successful approaching the problems of unsupervised and semi-supervised learning. Recently, the theory of graph signal processing and semi-supervised learning have been combined leading to new developments and insights in the field of machine learning. In this paper, concepts of recovery of graph signals and semi-supervised learning are introduced in the problem of background subtraction. We propose a new algorithm named GraphBGS, this method uses a Mask R-CNN for instances segmentation; temporal median filter for background initialization; motion, texture, color, and structural features for representing the nodes of a graph; k-nearest neighbors for the construction of the graph; and finally a semi-supervised method inspired from the theory of recovery of graph signals to solve the problem of background subtraction. The method is evaluated on the publicly available change detection, and scene background initialization databases. Experimental results show that GraphBGS outperforms unsupervised background subtraction algorithms in some challenges of the change detection dataset. And most significantly, this method outperforms generative adversarial networks in unseen videos in some sequences of the scene background initialization database.

1. Introduction

Background subtraction is an important topic in computer vision and video analysis. There are a large number of applications such as automatic surveillance of human activities in public spaces, intelligent transportation, video analysis, industrial vision, among others [47, 7]. Background subtraction aims to separate the moving objects, or foreground, from the static scene called background [5, 9]. This task is in general very difficult due to several challenges in the background, for instance: dynamic backgrounds, shadows, intermittent objects motion, scenes with bad weather, swaying leaves, water ripples, etc [15]. In this paper, the problem of background subtraction is addressed using con-

cepts of Graph Signal Processing (GSP).

Graphs provide the ability to model interactions of data residing on irregular and complex structures. Social, financial, and sensor networks are examples of data that can be modeled on graphs. GSP is thus an emerging field that extends the concepts of classical digital signal processing to signals supported on graphs [36, 39, 37, 29]. A graph signal is defined as a function over the nodes of a graph. The sampling and recovery of graph signals are fundamental tasks in GSP that have received considerable attention recently [12, 27, 45, 2, 35, 30]. In fact, the problem of semi-supervised learning can be modeled as the reconstruction of a graph signal from its samples [14, 2]. Currently, there is not any application of GSP in the field of background subtraction.

Deep learning models brought a breakthrough in the field of background subtraction since the performance of these algorithms is almost perfect [21]. However, there are still several open questions related to these deep learning-based methods: 1) most of the deep learning methods lack of theoretical guarantees, 2) deep learning background subtraction methods do not have good performance in unseen videos [13, 44], 3) besides the classical fundamental theorem of machine learning involving the VapnikChervonenkis dimension [46, 38], there is not a theoretical explanation about the sample complexity required in deep learning, 4) deep learning background subtraction methods involve similar images in training and evaluation (due to the nature of the problem). Then, there is not a real evaluation of the level of overfitting in these algorithms, specially when the amount of available information is not huge, as it is the case in background subtraction.

In this paper, the problem of background subtraction is addressed using reconstruction of graph signals. We proposed a new method called GraphBGS. This algorithm models the instances in the videos as nodes of a graph embedded in a high dimensional space. These instances are obtained using a Mask Region Convolutional Neural Network (Mask R-CNN) with a Residual Network of 50 layers (ResNet50) [16] plus Feature Pyramid Network (FPN) [22] as backbone. The Mask R-CNN is trained in the Common

Objects in Context (COCO) 2017 dataset [23]. The representation of the nodes is obtained using optical flow estimation, color, texture, and structural features in the instances. The graph is constructed with a k-nearest neighbors algorithm with $k = 10$. Furthermore, the task of the reconstruction algorithm is to classify whether or not an instance is a moving object, this semi-supervised algorithm is inspired by the variational approach of Pesenson [33]. Furthermore, the bandwidth of the graph signal offers a strong mathematical explanation for the sample complexity required in semi-supervised learning for a perfect classification [1], assuming no noise in the graph signal.

The main contribution of this paper are summarized as follow:

- Concepts of GSP are introduced for the first time in the field of background subtraction.
- Theorem 2 is introduced, showing the numerical stability of the semi-supervised algorithm in terms of a positive semi-definite perturbation matrix. The proof is given in Appendix A.
- The proposed algorithm outperforms several unsupervised background subtraction methods, and some of the supervised methods in some categories of the change detection database.
- The proposed algorithm outperforms the method of Bayesian generative adversarial networks [54] in terms of generalization in several videos of the scene background initialization dataset.

The rest of the paper is organized as follows. Section 2 presents the related works in background subtraction. Section 3 explains the notation, basic concepts, and the method GraphBGS. Section 4 introduces the experimental framework of this paper. Finally, Sections 5 and 6 present the results and conclusions, respectively.

2. Related Works

The state-of-the-art in background subtraction can be divided in unsupervised and supervised methods. For a complete review of unsupervised, and supervised methods the readers are referred to the survey papers [6, 5, 10, 8].

As far as we know, there are not algorithms in the state-of-the-art that use concepts of graph signal processing in the problem of background subtraction. However, some methods use concepts of semantic segmentation. For example, Braham *et al.* [11] proposed Semantic Background Subtraction (SemanticBGS) that uses algorithms of scene parsing [53] to improve any other unsupervised method of background subtraction. Zeng *et al.* [52] used the same idea of leveraging semantics to improve the performance of other unsupervised background subtraction algorithm, but in this case the method is designed to work in real time. Zeng *et al.* method has a feedback mechanism between the semantic segmentation algorithm and the unsupervised background

subtraction method. Braham *et al.* method has the advantage of being robust against dynamic backgrounds and shadows. However, SemanticBGS can be viewed as a post-processing step, and this algorithm fails when the unsupervised algorithm fails. For example, Braham *et al.* method is unable to improve the false negative rate of the original algorithm.

3. Background Subtraction via Reconstruction of Graph Signals

This section presents the notation and basic concepts of this paper, as well as the proposed background subtraction method. Figure 1 shows an overview of the pipeline of GraphBGS.

3.1. Notation

In this paper, upper case boldface letters such as \mathbf{W} represent matrices, and lower case boldface letters such as \mathbf{x} denote vectors. $\mathbf{Y}(i, :)$ is the i -th row vector of matrix \mathbf{Y} . $(\cdot)^T$ represents transposition. $\sigma_{\max}(\mathbf{A})$ and $\sigma_{\min}(\mathbf{A})$ represent the maximum and minimum singular values of the matrix \mathbf{A} , respectively. Calligraphic letters such as \mathcal{V} denote sets, and $|\mathcal{V}|$ represents its cardinality. $\text{diag}(\mathbf{x})$ is a diagonal matrix with entries x_1, x_2, \dots, x_n . Finally, $\mathbf{1}_{\mathcal{A}} : \mathcal{X} \rightarrow \{0, 1\}$ is the indicator function of a subset $\mathcal{A} \subset \mathcal{X}$ defined as:

$$\mathbf{1}_{\mathcal{A}}(x) \triangleq \begin{cases} 1 & \text{if } x \in \mathcal{A}, \\ 0 & \text{if } x \notin \mathcal{A}, \end{cases} \quad (1)$$

3.2. Background

Let $G = (\mathcal{V}, \mathcal{E})$ be an undirected, weighted, and connected graph; where $\mathcal{V} = \{1, \dots, N\}$ is the set of N nodes and $\mathcal{E} = \{(i, j)\}$ is the set of edges. The 2-tuple (i, j) stands for an edge between two nodes i and j . $\mathbf{W} \in \mathbb{R}^{N \times N}$ is the adjacency matrix of the graph such that $\mathbf{W}(i, j) = w_{ij} \in \mathbb{R}^+$ is the weight between nodes i and j . As a consequence, \mathbf{W} is symmetric for undirected graphs. A graph signal is a function $x : \mathcal{V} \rightarrow \mathbb{R}$ defined on the nodes of G , and can be represented as $\mathbf{x} \in \mathbb{R}^N$ where $\mathbf{x}(i)$ is the function evaluated on the i th node. Furthermore, $\mathbf{D} \in \mathbb{R}^{N \times N}$ is a diagonal matrix called the degree matrix of the graph such that $\mathbf{D}(i, i) = \sum_{j=1}^N \mathbf{W}(i, j) \forall i = 1, 2, \dots, N$. Likewise, the combinatorial Laplacian operator is a positive semi-definite matrix defined as $\mathbf{L} = \mathbf{D} - \mathbf{W}$, and it has eigenvalues $0 = \lambda_1 \leq \lambda_2 \leq \dots \leq \lambda_N$ and corresponding eigenvectors $\{\mathbf{u}_1, \mathbf{u}_2, \dots, \mathbf{u}_N\}$.

The graph Fourier basis of G is defined by the spectral decomposition of $\mathbf{L} = \mathbf{U}\mathbf{\Lambda}\mathbf{U}^T$, where $\mathbf{U} = [\mathbf{u}_1, \mathbf{u}_2, \dots, \mathbf{u}_N]$ and $\mathbf{\Lambda} = \text{diag}(\lambda_1, \lambda_2, \dots, \lambda_N)$. Therefore, the Graph Fourier Transform (GFT) $\hat{\mathbf{x}}$ of the signal \mathbf{x} is defined as $\hat{\mathbf{x}} = \mathbf{U}^T \mathbf{x}$, and the inverse GFT is

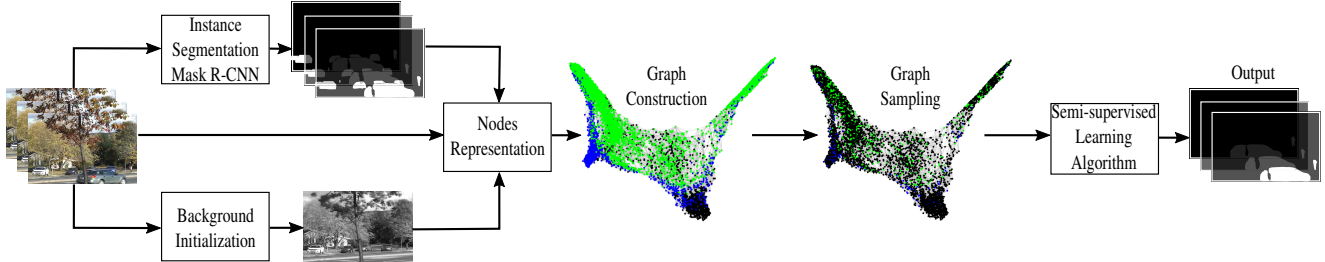


Figure 1. Pipeline of the background subtraction method via recovery of graph signals. GraphBGS uses a temporal median filter [34] as background initialization, and the instances are obtained using Mask R-CNN [16]. Each instance represents a node in the graph, and the representation of each node is obtained with motion, color, texture, and structural features. Green and blue nodes correspond to moving and static objects, respectively. Black nodes correspond to non-labeled instances in the database. Finally, some nodes are sampled and the semi-supervised algorithm reconstructs all the labels in the graph.

given by $\mathbf{x} = \mathbf{U}\hat{\mathbf{x}}$. Using this notion of frequency, Peerson [32] defined the space of all ω -bandlimited signals as $PW_\omega(G) = \text{span}(\mathbf{U}_k : \lambda_k \leq \omega)$, where \mathbf{U}_k represents the first k eigenvectors of \mathbf{L} , and $PW_\omega(G)$ is known as the Paley-Wiener space of G . As a consequence, a graph signal \mathbf{x} has cutoff frequency ω , and bandwidth k if $\mathbf{x} \in PW_\omega(G)$.

Given the notion of bandlimitedness in terms of $PW_\omega(G)$, the next step is to find a bound for the minimum sampling rate allowing perfect recovery of graph signals $\mathbf{x} \in PW_\omega(G)$. In other words, what is the minimum amount of labels required to have perfect classification in semi-supervised learning, given the prior assumption that the classes of the nodes lie in the Paley-Wiener space of the graph? The answer to this question is that one needs at least k (bandwidth) labels to get a perfect classification. Intuitively, a graph signal \mathbf{x} is smooth when $\mathbf{x} \in PW_\omega(G)$. For instance, suppose a temperature sensor network in any region of the world. The temperature of two nearby cities or localities, represented as the value of a graph signal in two nodes, should be similar. Then, probably one just needs one of the values of temperature to guess the value of the signal in the other node.

Formally, the sampling rate of a graph signal is defined in terms of a subset of nodes $\mathcal{S} \subset \mathcal{V}$ with $\mathcal{S} = \{s_1, s_2, \dots, s_m\}$, where $m = |\mathcal{S}| \leq N$ is the number of sampled nodes. The sampled graph signal is defined as $\mathbf{x}(\mathcal{S}) = \mathbf{M}\mathbf{x}$, where \mathbf{M} is a binary decimation matrix whose entries are given by $\mathbf{M} = [\delta_{s_1}, \dots, \delta_{s_m}]^T$ and δ_v is the N -dimensional Kronecker column vector centered at v . The reconstruction of the graph signal is achieved as $\mathbf{x}' = \Phi\mathbf{M}\mathbf{x}$, where $\Phi \in \mathbb{R}^{N \times m}$ is an interpolation operator. Perfect reconstruction happens when $\Phi\mathbf{M}$ is the identity matrix. This is not possible in general since $\text{rank}(\Phi\mathbf{M}) \leq m \leq N$. However, perfect recovery from $\mathbf{x}(\mathcal{S})$ is possible if the sampling size $|\mathcal{S}|$ is greater than or equal to k , i.e., $|\mathcal{S}| \geq k$ [12].

Theorem 1 (Chen’s theorem [12]). *Let \mathbf{M} satisfies $\text{rank}(\mathbf{M}\mathbf{U}_k) = k$. For all $\mathbf{x} \in PW_\omega(G)$, perfect recovery*

is achieved by choosing:

$$\Phi = \mathbf{U}_k \mathbf{V}, \quad (2)$$

with $\mathbf{V}\Phi\mathbf{U}_k$ a $k \times k$ identity matrix.

Proof: see [12].

Theorem 1 indicates that perfect classification in semi-supervised learning is possible when the classes of the problem lie in the Paley-Wiener space of the graph, and the number of sampling nodes is at least k . This classification is achieved by choosing the interpolation operator as in Eqn. 2. The computation of the Laplacian eigenvectors in Eqn. 2 is computationally prohibitive for large graphs. In this paper, the computation of the Laplacian eigenvectors is avoided. For further details, please see Section 3.7.

3.3. Instance Segmentation

The instance segmentation is obtained using Mask R-CNN [16] with a ResNet50 [17] plus FPN [22] as backbone. This network uses fully connected layers for mask prediction. The model for instance segmentation was trained in the COCO dataset 2017 [23]. Each mask-output of the instance segmentation network is a node in the proposed background subtraction method. However, since there are classes in the COCO dataset that are probably static objects, GraphBGS discards the following objects to reduce computational complexity: traffic light, fire hydrant, stop sign, parking meter, bench, chair, couch, potted plant, bed, dining table, toilet, tv, microwave, oven, toaster, sink, refrigerator, clock, vase.

The instance segmentation network gives a fundamental limitation to GraphBGS: if the Mask R-CNN do not segment a moving object, GraphBGS will not be able to detect it. As a consequence, the proposed method has an upper bound in the performance. This upper bound is known when the classification algorithm has the label of every node in the graph. A discussion about the upper bounds is presented in Section 5.

3.4. Background Estimation and Nodes Representation

For the sake of simplicity, the computation of the background image is performed using the temporal median filter [34]. However, most advanced methods in background initialization such as [18, 51] could be used to improve the overall performance of the algorithm. The videos are processed in gray-scales in this paper.

The representation of the nodes are obtained using optical flow estimation, color, texture, and structural features. First of all, Lucas-Kanade method [24] is used to estimate the optical flow between consecutive frames in the video, and also between each frame and the background. The representation of the motion in each node is obtained computing histograms of the vertical and horizontal velocities, orientation, and magnitude of the optical flow, as well as some descriptive statistics (the minimum, maximum, mean, standard deviation, mean absolute deviation, and range). The color features are obtained computing the normalized histogram of the gray-scaled pixels of the instance. The texture representation is obtained calculating the local binary patterns [28] of each instance. Finally, the structural features are obtained computing the eccentricity, Euler number, extent, orientation, solidity, and the ratio between the number of pixels of the instance and the total number of pixels in the image. The representation of the node is obtained concatenating all the previous features, *i.e.*, motion, color, texture, and structural features. Each instance is represented by a 930-dimensional vector.

3.5. Graph Construction

Let $\mathbf{X} \in \mathbb{R}^{N \times M}$ be the matrix of N instances, in which each instance is a M -dimensional vector ($M = 930$, for further details see Section 3.4). Firstly, a k -nearest neighborhood algorithm with $k = 10$ is used to connect the nodes in the graph. Afterwards, vertices are connected to get an undirected graph. The weight between two connected nodes i, j is given such that $w_{ij} = \exp -\frac{d(i,j)^2}{\sigma^2}$, where $d(i, j) = \|\mathbf{X}(i, :) - \mathbf{X}(j, :)\|$, and σ^2 is the standard deviation of the Gaussian function computed as:

$$\sigma = \frac{1}{|\mathcal{E}| + N} \sum_{(i,j) \in \mathcal{E}} d(i, j). \quad (3)$$

3.6. Graph Signal

Since this is a classification problem, the graph signal is a matrix $\mathbf{Y} \in \mathbb{R}^{N \times Q}$, where Q is the number of classes of the problem. In this paper, the graph signal is given by the membership function \mathbf{Y}^c of each class c which takes a value of 1 on a node which belongs to the class and is 0 otherwise, *i.e.*, Q is equal to 2 corresponding to the classes "background" [1, 0] and "foreground" [0, 1]. The decision

of whether a node is background or foreground is based on a comparison between the ground-truth and the instances of the videos. The proposed method uses the following metrics to determine the foreground and background nodes: Intersection over Union (IoU), and Intersection over Node (IoN). Each output of the Mask R-CNN is represented by a set of indexes \mathcal{N} in the image, and each isolated region of the ground-truth is represented by a set of indexes \mathcal{GT} in the image. Intersection over union is defined as:

$$IoU = \frac{\sum_{i=1}^{|\mathcal{U}|} \mathbf{1}_{\mathcal{I}}(i)}{|\mathcal{U}|}, \quad (4)$$

where $\mathcal{U} = \mathcal{GT} \cup \mathcal{N}$, $\mathcal{I} = \mathcal{GT} \cap \mathcal{N}$, $\mathcal{I} \subset \mathcal{U}$, and $\mathbf{1}_{\mathcal{I}}$ is the indicator function of the subset $\mathcal{I} \subset \mathcal{U}$. Furthermore, intersection over node is defined as:

$$IoN = \frac{\sum_{i=1}^{|\mathcal{U}|} \mathbf{1}_{\mathcal{I}}(i)}{|\mathcal{N}|}. \quad (5)$$

Each output of the Mask R-CNN is compared with every isolated region in the corresponding ground-truth image. As a consequence, each instance is characterized by a scalar IoN , and a vector $\mathbf{u} \in \mathbb{R}^\alpha$, where α corresponds to the number of isolated regions in the ground truth image, and $\mathbf{u}(i)$ is the IoU between the segmented-instance and the i -th region in the corresponding ground-truth image for all $i = 1, 2, \dots, \alpha$. The graph signal \mathbf{Y} is constructed as follow, for all $j = 1, 2, \dots, N$:

$$\mathbf{Y}(j, :) = \begin{cases} [1, 0] & \text{if } \mathbf{u}^j \in \emptyset, \\ [0, 1] & \text{if } \max(\mathbf{u}^j) > 0.25, \\ [0, 1] & \text{if } IoN > 0.45 \text{ AND} \\ & \max(\mathbf{u}^j) > 0.05, \\ [0, 1] & \text{if } IoN > 0.9 \text{ AND} \\ & \max(\mathbf{u}^j) > 0.02, \\ [1, 0] & \text{Otherwise,} \end{cases} \quad (6)$$

where \mathbf{u}^j is the vector of IoU 's of the j -th instance. This procedure is fundamentally empiric, however it can be done manually by looking at each instance and its intersection with the ground-truth, or it can be done with some algorithm of machine learning (by learning the parameters).

3.7. Semi-supervised Learning Algorithm

The semi-supervised learning algorithm is based on the variational splines of Pesenson [33].

Definition 1. Let $\mathbf{g}^*(v)$ be the complex conjugate of $\mathbf{g}(v)$. The space $L_2(G)$ is the Hilbert space of all complex-valued functions $\mathbf{f} : \mathcal{V} \rightarrow \mathbb{C}$ in the graph G with the following inner product:

$$\langle \mathbf{f}, \mathbf{g} \rangle = \sum_{v \in \mathcal{V}} \mathbf{f}(v) \mathbf{g}^*(v) \mathbf{D}(v, v), \quad (7)$$

and $\|\mathbf{f}\| = \|\mathbf{f}\|_0 = (\sum_{v \in \mathcal{V}} |\mathbf{f}(v)|^2 \mathbf{D}(v, v))^{1/2}$.

Definition 2. For a fixed $\epsilon \geq 0$ the Sobolev norm is introduced by the following formula:

$$\|\mathbf{f}\|_{t, \epsilon} = \|(\epsilon \mathbf{I} + \mathbf{L})^{t/2} \mathbf{f}\|, t \in \mathbb{R}. \quad (8)$$

Let \mathbf{z}_q and $\mathbf{y}_q(\mathcal{S})$ be the reconstructed and the sampled graph signals associated to the q -th class, respectively. Given a subset of vertices $\mathcal{S} \subset \mathcal{V}$, a sampled vector of labels $\mathbf{y}_q(\mathcal{S}) = \mathbf{M}\mathbf{y}_q$, a positive $t > 0$, and a non-negative $\epsilon \geq 0$, the variational problem for semi-supervised learning is stated as follow: find a vector \mathbf{z}_q from the space $L_2(G)$ with the following properties: $\mathbf{z}_q(\mathcal{S}) = \mathbf{M}\mathbf{z}_q = \mathbf{y}_q(\mathcal{S})$, and \mathbf{z}_q minimizes functional $\mathbf{z}_q \rightarrow \|(\epsilon \mathbf{I} + \mathbf{L})^{t/2} \mathbf{z}_q\|$. In other words, the variational problem is trying to solve the following optimization problem:

$$\begin{aligned} \arg \min_{\mathbf{z}_q} \|\mathbf{z}_q\|_{t, \epsilon} \quad \text{s.t.} \quad \mathbf{M}\mathbf{z}_q = \mathbf{y}_q(\mathcal{S}) \rightarrow \\ \arg \min_{\mathbf{z}_q} \mathbf{z}_q^\top (\epsilon \mathbf{I} + \mathbf{L})^t \mathbf{z}_q \quad \text{s.t.} \quad \mathbf{M}\mathbf{z}_q - \mathbf{y}_q(\mathcal{S}) = 0, \end{aligned} \quad (9)$$

for $q = 1, 2$. Equation 9 is a convex optimization problem since the term $\mathbf{z}_q^\top (\epsilon \mathbf{I} + \mathbf{L})^t \mathbf{z}_q$ is a quadratic convex function; and the term $\mathbf{M}\mathbf{z}_q - \mathbf{y}_q(\mathcal{S})$ is affine in \mathbf{z}_q . Moreover, the optimization problem in Eqn. 9 has a closed-form solution for $t > 0$ given by:

$$\mathbf{Z}_{\text{rec}} = ((\epsilon \mathbf{I} + \mathbf{L})^{-1})^t \mathbf{M}^\top (\mathbf{M}((\epsilon \mathbf{I} + \mathbf{L})^{-1})^t \mathbf{M}^\top)^{-1} \mathbf{Y}(\mathcal{S}), \quad (10)$$

where $\mathbf{Z}_{\text{rec}} = [\mathbf{z}_1, \mathbf{z}_2]$. Even though $\det(\mathbf{L}) = 0$ for undirected, and connected graphs, the term $(\epsilon \mathbf{I} + \mathbf{L})^{-1}$ is always invertible for $\epsilon > 0$. Intuitively, the value ϵ is related to the stability of the inverse of $(\mathbf{L} + \epsilon \mathbf{I})$.

Theorem 2. Given an undirected, connected graph G with combinatorial Laplacian matrix \mathbf{L} such that $\text{rank}(\mathbf{L}) = N - 1$, and let $\mathbf{\Psi} \in \mathbb{R}^{N \times N}$ a perturbation matrix. The summation $\mathbf{L} + \mathbf{\Psi}$ has a lower and upper bound in the condition number in the ℓ_2 -norm such that:

$$\frac{\sigma_{\max}(\mathbf{L} + \mathbf{\Psi})}{\sigma_{\max}(\mathbf{\Psi})} \leq \kappa(\mathbf{L} + \mathbf{\Psi}) \leq \frac{\sigma_{\max}(\mathbf{L}) + \sigma_{\max}(\mathbf{\Psi})}{\sigma_{\min}(\mathbf{L} + \mathbf{\Psi})}, \quad (11)$$

where $\kappa(\mathbf{L} + \mathbf{\Psi})$ is the condition number of $\mathbf{L} + \mathbf{\Psi}$.

Proof: see Appendix A.

Theorem 2 provides a lower and upper bound in the condition number¹ of $\mathbf{L} + \mathbf{\Psi}$. The lower bound can be achieved by computing the GFT of \mathbf{L} . The addition of a perturbation matrix to the Laplacian matrix is implicitly changing the eigenvalues of \mathbf{L} , however Theorem 2 does not state how the eigenvalues of \mathbf{L} change. In matrix theory, Weyl's inequality [49] is a theorem about how the eigenvalues of a perturbed matrix change.

¹The condition number $\kappa(\mathbf{A})$ associated with the square matrix \mathbf{A} is a measure of how well or ill conditioned is the inversion of \mathbf{A} .

Theorem 3 (Weyl's Theorem [49]). Let \mathbf{L} and $\mathbf{\Psi}$ be Hermitian matrices with set of eigenvalues $\{\lambda_1, \lambda_2, \dots, \lambda_N\}$ and $\{\psi_1, \psi_2, \dots, \psi_N\}$, respectively. The matrix $\mathbf{L}_{\text{per}} = \mathbf{L} + \mathbf{\Psi}$ has a set of eigenvalues $\{\nu_1, \nu_2, \dots, \nu_N\}$ where the following inequalities hold for $i = 1, 2, \dots, N$:

$$\lambda_i + \psi_1 \leq \nu_i \leq \lambda_i + \psi_N. \quad (12)$$

Proof: see [49].

In Theorem 3, if $\mathbf{\Psi} \succ \mathbf{0}$, i.e. $\psi_i > 0 \forall 1 \leq i \leq N$, then this implies that $\nu_i > \lambda_i \forall i = 1, 2, \dots, N$. Weyl's Theorem indicates how the eigenvalues of \mathbf{L} change after adding a perturbation matrix, and it gives insights about the structure of $\mathbf{\Psi}$. It is desirable to have $\det(\mathbf{L}_{\text{per}}) \neq 0$, then $\mathbf{\Psi}$ should be positive definite. Assuming $\mathbf{\Psi} = \epsilon \mathbf{I}$, where $\epsilon \in \mathbb{R}^+$ and \mathbf{I} is the identity matrix, we have $\sigma_{\max}(\mathbf{\Psi}) = \epsilon$. Furthermore, the minimum eigenvalue σ_{\min} of $\mathbf{L} + \mathbf{\Psi}$ is strictly greater than zero according to Theorem 3, i.e. $\nu_1 > \lambda_1$, since $\sigma_{\min}(\mathbf{L} + \mathbf{\Psi}) > 0$ the upper bound in Eqn. 11 is:

$$\kappa(\mathbf{L} + \mathbf{\Psi}) \leq \frac{\sigma_{\max}(\mathbf{L}) + \epsilon}{\sigma_{\min}(\mathbf{L} + \mathbf{\Psi})} < \infty. \quad (13)$$

The term $(\epsilon \mathbf{I} + \mathbf{L})$ is precisely the first term in the Sobolev norm in Eqn. 8, and the invertible term in the variational problem in Eqn. 9. ϵ is fundamentally related to how well conditioned is the variational problem. Larger values of ϵ leads to better condition numbers, but also to larger changes of the eigenvalues of the Laplacian matrix. Experimentally, ϵ is set to 0.2. The final classification $\hat{\mathbf{Y}}(i, \cdot)$ of node i is obtained such as:

$$\hat{\mathbf{Y}}(i, \cdot) = \arg \max_c \{\mathbf{Z}_{\text{rec}}^c(i, \cdot)\} \forall i \in \mathcal{V}. \quad (14)$$

The optimization problem in Eqn. 9 is solved using the graph signal processing toolbox [31].

4. Experimental Framework

This section introduces the databases used in this paper, the evaluation metrics, the experiments, and the implementation details of GraphBGS.

4.1. Databases

The Change Detection (CDNet2014)² [15], and the Scene Background Initialization (SBI)³ datasets [26] were used in this paper. CDNet2014 contains 11 challenges: bad weather, low frame rate, night videos, PTZ, turbulence, baseline, dynamic background, camera jitter, intermittent object motion, shadow, and thermal. Each challenge contains from 4 up to 6 videos, and each video has from 600 up to 7999 frames. Every video contains a certain amount

²<http://www.changedetection.net>

³<http://sbmi2015.na.icar.cnr.it/SBIdataset.html>

of ground-truth frames, in which the ground truth shows the foreground and background. In the other hand, SBI dataset contains 14 video sequences, this dataset was originally created to test background initialization algorithms. However, Wang *et al.* [48] provides the ground-truth for background subtraction for the SBI in their paper.

4.2. Evaluation Metrics

The F-measure, recall, and precision are the metrics used to compare GraphBGS with the state-of-the-art methods. Recall and precision metrics are defined as follow:

$$\text{Recall} = \frac{\text{TP}}{\text{TP} + \text{FN}}, \quad (15)$$

$$\text{Precision} = \frac{\text{TP}}{\text{TP} + \text{FP}}, \quad (16)$$

where TP, FP, and FN are the number of True Positives, False Positives, and False Negatives pixels, respectively. Finally the F-measure is defined as:

$$\text{F-measure} = 2 \frac{\text{Precision} \times \text{Recall}}{\text{Precision} + \text{Recall}}. \quad (17)$$

4.3. Experiments

There are two experiments in this paper, the first one is related to the CDNet2014 dataset. Moreover, there is an experiment related to the generalization to unseen of GraphBGS in the SBI database. In the first experiment, a graph is constructed for each challenge in the CDNet2014. Then, a percentage of the amount of frames (sampling density) in each sequence is extracted, *i.e.*, this amount of image is sampled in the graph. Finally, the reconstruction algorithm is performed to classify the non-labeled frames. This procedure is repeated 5 times for each sampling density (this procedure is called Monte Carlo cross-validation in the literature of machine learning).

The second experiment constructs a graph with the whole SBI dataset and the challenges baseline, dynamic background, and shadow from the CDNet2014 database. In this case, a percentage of the frames is extracted from each sequence, excluding all the sequences of SBI dataset. In other words, the second experiment is testing the generalization power of the method in unseen videos. The metrics in both experiments are computed in the non-sampled images.

4.4. Implementation Details

The instance segmentation algorithm was implemented using Pytorch and Detectron2 [50]. The construction of the graph, and the algorithm for reconstruction of graph signals were implemented using the graph signal processing toolbox [31]. For the second experiment, SuBSENSE was implemented using the BGSLibrary [40].

The processing time of GraphBGS is 1.81 Frames Per Second (FPS) for a 320×240 video. The Mask R-CNN was executed on a Tesla K80 GPU (at 2.78 FPS). The rest of the method was executed on a laptop with a CPU Intel Core i7 – 3630QM and 8 GB of memory RAM (at 5.21 FPS).

5. Results and Discussion

In the first experiment, our semi-supervised algorithm GraphBGS is compared with some state-of-the-art unsupervised methods including: GMM [43], SC-SOBS [25], SuBSENSE [41], and PAWCS [42]. The experiments omit the results of post-processing algorithms such as IUTIS [4] and SemanticBGS [11] since they can be applied to any other background subtraction algorithm, including GraphBGS, to improve its performance. The supervised methods DeepBS [3] and BSPVGAN [54] are also displayed in the results for reference. In the second experiment, GraphBGS is compared against SuBSENSE [41] and BSPVGAN [54]. Table 1 shows some visual results of our algorithm compared with SuBSENSE [41], PAWCS [42], and BSPVGAN [54].

Figure 2 shows the results of the first experiment in nine challenges of the change detection 2014 dataset with its corresponding upper bound in performance for the GraphBGS method. This experiment constructs a graph for each challenge. The gap between the upper bound and the average f-measure provides information about GraphBGS in each challenge. For example, the performance could be improved by enhancing the instance segmentation algorithm when the upper bound and the average f-measure is very close, as it is the case in the challenges "baseline", "shadow", "thermal", "dynamic background", and "intermittent object motion". In the other hand, if the average f-measure is far from the upper bound, one should either improve: the representation of the nodes, the background initialization algorithm, or the semi-supervised learning algorithm. This is the case with the challenges "camera jitter", "low frame rate", "PTZ", and "bad weather" in Figure 2.

Table 2 shows the results of the first experiment in the CDNet2014 database. The results of categories "turbulence" and "night videos" are not displayed since Mask R-CNN fails to segment some of the videos. As a consequence, it is not possible to detect the moving objects in some sequences for the semi-supervised learning algorithm. Since the experiments perform cross-validation, the results of our method show the mean of the averages f-measure, recall, and precision. In the other hand, Table 3 shows the results of the second experiment in some videos of the SBI dataset related to the generalization power of GraphBGS. The results of BSPVGAN in this experiment come from their paper [54].

In the first experiment, GraphBGS outperforms the unsu-

Table 1. Some visual results on CDNet2014 dataset compared with state-of-the-art algorithms, from left to right: original images, ground-truth images, PAWCS [42], SuBSENSE [41], BSPVGAN [54], and the proposed GraphBGS algorithm.

Categories	Original	Ground Truth	PAWCS	SuBSENSE	BSPVGAN	GraphBGS (ours)
Bad Weather Snow Fall in002776						
Baseline PETS2006 in000986						
Camera Jitter Badminton in000980						
Dynamic-B Fall in002795						
I-O- Motion, Sofa in002795						

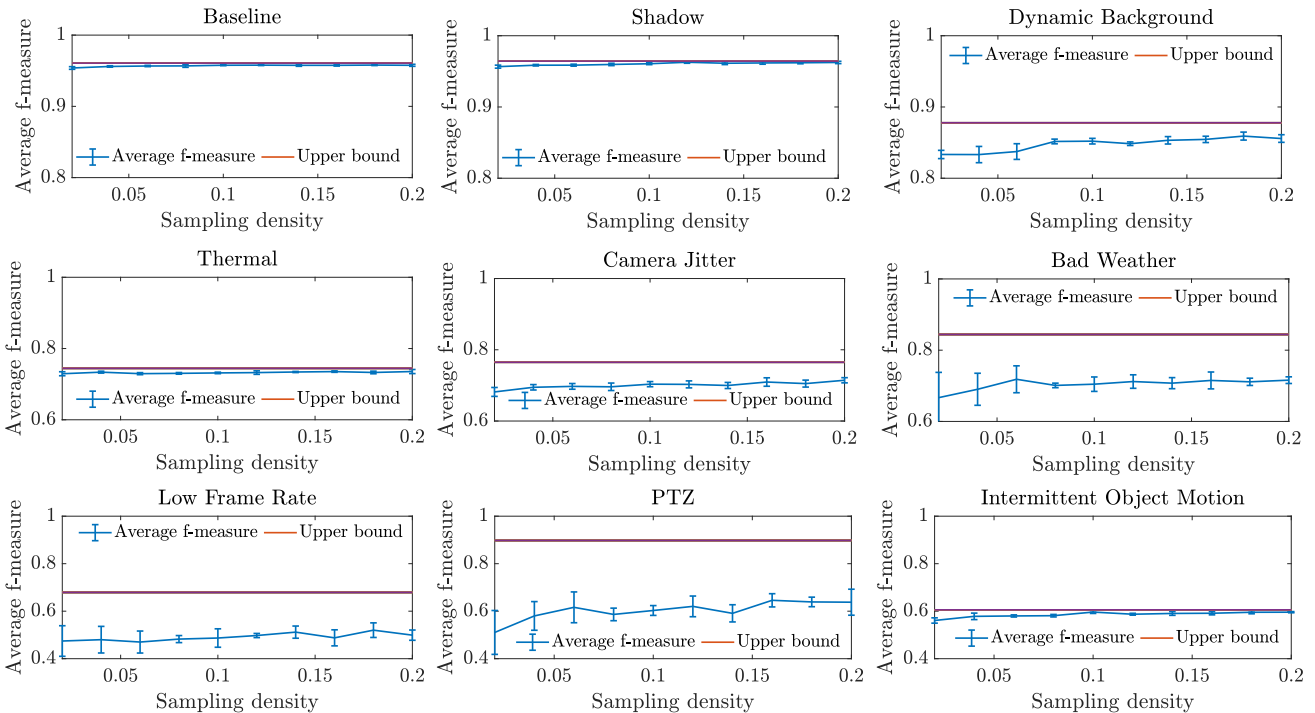


Figure 2. Average f-measure (with standard deviation) vs sampling density, and upper bound in the performance of 9 challenges of the CDNet2014 dataset. Each point in each plot is a Monte Carlo cross validation experiment with 5 repetitions.

pervised methods in the challenges: "baseline", "shadow", and "PTZ" in the f-measure metric; "shadow" in the recall

metric; and "baseline", "intermittent object motion", "low frame rate", "PTZ", and "shadow" in the precision metric.

Table 2. Average f-measure, recall, and precision results over 9 challenges of the CDNet2014, namely: bad weather (BWT), baseline (BSL), camera jitter (CJI), dynamic background (DBA), intermittent object motion (IOM), low frame rate (LFR), PTZ, shadow (SHW), and thermal (THL). GraphBGS is compared with 6 algorithms of the state-of-the-art. The best performance in each metric with respect to unsupervised methods is in **bold**. The algorithms from the state-of-the-art are: GMM [43], SC-SOBS [25], SuBSENSE [41], PAWCS [42], DeepBS [3], and BSPVGAN [54]. The results of the state-of-the-art methods come from the change detection website.

Method	BWT	BSL	CJI	DBA	IOM	LFR	PTZ	SHW	THL	Overall
Average f-Measure										
GMM (unsupervised)	0.738	0.824	0.597	0.633	0.521	0.537	0.152	0.737	0.662	0.600
SC-SOBS (unsupervised)	0.662	0.933	0.705	0.669	0.592	0.546	0.041	0.779	0.692	0.624
SuBSENSE (unsupervised)	0.862	0.950	0.815	0.818	0.657	0.644	0.348	0.899	0.817	0.757
PAWCS (unsupervised)	0.815	0.940	0.814	0.894	0.776	0.659	0.461	0.891	0.832	0.787
GraphBGS (semi, ours)	0.718	0.958	0.714	0.851	0.596	0.520	0.646	0.963	0.735	0.744
DeepBS (supervised)	0.830	0.958	0.899	0.876	0.610	0.600	0.313	0.930	0.758	0.753
BSPVGAN (supervised)	0.964	0.983	0.989	0.984	0.936	0.851	0.949	0.985	0.975	0.957
Average recall										
GMM (unsupervised)	0.718	0.818	0.733	0.834	0.514	0.582	0.647	0.796	0.569	0.690
SC-SOBS (unsupervised)	0.568	0.933	0.811	0.892	0.724	0.787	0.840	0.850	0.600	0.778
SuBSENSE (unsupervised)	0.821	0.952	0.824	0.777	0.658	0.854	0.831	0.941	0.816	0.830
PAWCS (unsupervised)	0.718	0.941	0.784	0.887	0.749	0.773	0.698	0.917	0.850	0.813
GraphBGS (semi, ours)	0.589	0.950	0.644	0.877	0.500	0.408	0.520	0.952	0.664	0.678
DeepBS (supervised)	0.752	0.952	0.879	0.854	0.573	0.592	0.746	0.958	0.664	0.774
BSPVGAN (supervised)	0.957	0.991	0.990	0.993	0.914	0.863	0.979	0.987	0.976	0.961
Average precision										
GMM (unsupervised)	0.770	0.846	0.513	0.599	0.669	0.689	0.118	0.716	0.865	0.643
SC-SOBS (unsupervised)	0.843	0.934	0.629	0.628	0.590	0.527	0.021	0.723	0.886	0.642
SuBSENSE (unsupervised)	0.909	0.950	0.811	0.891	0.796	0.603	0.284	0.865	0.833	0.771
PAWCS (unsupervised)	0.947	0.939	0.866	0.904	0.839	0.640	0.472	0.871	0.828	0.812
GraphBGS (semi, ours)	0.942	0.966	0.846	0.879	0.927	0.741	0.945	0.978	0.862	0.898
DeepBS (supervised)	0.968	0.966	0.931	0.908	0.825	0.702	0.285	0.909	0.926	0.824
BSPVGAN (supervised)	0.972	0.977	0.988	0.979	0.965	0.843	0.921	0.982	0.977	0.956

Table 3. F-measure, recall, and precision results over 9 sequences of the SBI dataset, namely: Board (BRD), CAVIAR1 (CA1), CAVIAR2 (CA2), HallAndMonitor (HAM), HighwayI (HGI), HighwayII (HGII), HumanBody2 (HB2), IBLtest2 (IB2), and Toscana (TOS). GraphBGS is compared in generalization with 2 algorithms of the state-of-the-art. The best performance in each metric for each sequence is in **bold**. The algorithms from the state-of-the-art are: SuBSENSE [41] and BSPVGAN [54].

Method	BRD	CA1	CA2	HAM	HGI	HGII	HB2	IB2	TOS	Overall
F-Measure										
SuBSENSE (unsupervised)	0.660	0.877	0.876	0.755	0.509	0.878	0.856	0.928	0.824	0.796
BSPVGAN (supervised)	0.953	0.944	0.917	0.902	0.924	0.915	0.916	0.926	0.935	0.926
GraphBGS (semi, ours)	0.981	0.987	0.773	0.954	0.848	0.814	0.965	0.979	0.938	0.915
Recall										
SuBSENSE (unsupervised)	0.515	0.921	0.893	0.660	0.531	0.860	0.814	0.910	0.914	0.780
BSPVGAN (supervised)	0.953	0.947	0.903	0.904	0.927	0.930	0.938	0.931	0.943	0.931
GraphBGS (semi, ours)	0.966	0.981	0.847	0.917	0.741	0.691	0.945	0.965	0.896	0.883
Precision										
SuBSENSE (unsupervised)	0.921	0.837	0.859	0.834	0.489	0.897	0.902	0.948	0.750	0.826
BSPVGAN (supervised)	0.954	0.942	0.931	0.901	0.922	0.901	0.895	0.921	0.927	0.921
GraphBGS (semi, ours)	0.995	0.994	0.711	0.993	0.991	0.989	0.986	0.993	0.985	0.960

In the second experiment, GraphBGS method outperforms almost all the algorithms in the tested sequences. The results in the metric precision suggest that GraphBGS is robust against false positives. However, the algorithm should

be improved with respect to the false negatives as noted by the relatively poor results in recall. This could be achieved by improving the segmentation algorithm, the background initialization method, the semi-supervised learning algo-

algorithm, and probably the representation of the nodes. Even though GraphBGS is a very simple method (temporal median filter, optical flow estimation, local binary patterns) the results are promising. This method could be the first of several semi-supervised learning algorithms that exploit concepts of GSP in the field of background subtraction.

6. Conclusions

This paper introduced a method for background subtraction based on the theory of reconstruction of graph signals. The pipeline of the method involves a Mask R-CNN as instance segmentation method; median filter as background initialization; motion, color, texture, and structural features for the representation of the nodes in a graph; a k-nearest neighbors for the construction of the graph; and finally a semi-supervised learning algorithm based on reconstruction of graph signals. This method outperforms unsupervised methods in some categories of the CDNet2014 database. But most important, this method outperforms a generative adversarial network method in unseen videos.

The present work opens up some new questions for future research. What is the role of graphs and the structure of a given dataset to improve the generalization of current deep learning methods? What is the relationship between the sampling of graph signals and the problem of background subtraction? Perhaps, concepts of graph signal processing such as active semi-supervised learning [1], learning graphs from data [20], and graph convolutional neural networks [19] could improve the performance of the algorithms in the field of background subtraction.

Appendices

A. Proof Theorem Perturbation Matrix

Proof. For simplicity, and without loss of generality consider the combinatorial Laplacian matrix $\mathbf{L} \in \mathbb{R}^{N \times N}$ of G such that $\text{rank}(\mathbf{L}) = N - 1$, i.e. \mathbf{L} is ill-conditioned. Since \mathbf{L} does not have full rank $\exists \mathbf{x} \neq \mathbf{0} \mid \mathbf{L}\mathbf{x} = \mathbf{0}$. Then:

$$\begin{aligned} (\mathbf{L} + \Psi)\mathbf{x} &= \Psi\mathbf{x} \\ \|(\mathbf{L} + \Psi)\mathbf{x}\|_2 &= \|\Psi\mathbf{x}\|_2 \\ \frac{\|(\mathbf{L} + \Psi)\mathbf{x}\|_2}{\|\mathbf{x}\|_2} &= \frac{\|\Psi\mathbf{x}\|_2}{\|\mathbf{x}\|_2}, \end{aligned} \quad (18)$$

where $\Psi \in \mathbb{R}^{N \times N}$ is a perturbation matrix.

Lemma 4. *If $\|\cdot\|$ is a matrix norm induced by a vector norm $\|\cdot\|$, then:*

$$\|\mathbf{A}\mathbf{x}\| \leq \|\mathbf{A}\| \cdot \|\mathbf{x}\|. \quad (19)$$

Proof. Since $\|\mathbf{A}\| = \max_{\mathbf{x} \neq \mathbf{0}} \frac{\|\mathbf{A}\mathbf{x}\|}{\|\mathbf{x}\|}$, for an arbitrary $\mathbf{y} \in \mathbb{R}^N$, with $\mathbf{y} \neq \mathbf{0}$:

$$\begin{aligned} \|\mathbf{A}\| &= \max_{\mathbf{x} \neq \mathbf{0}} \frac{\|\mathbf{A}\mathbf{x}\|}{\|\mathbf{x}\|} \geq \frac{\|\mathbf{A}\mathbf{y}\|}{\|\mathbf{y}\|} \\ &\rightarrow \|\mathbf{A}\mathbf{y}\| \leq \|\mathbf{A}\| \cdot \|\mathbf{y}\|. \end{aligned} \quad (20)$$

This also holds true for $\mathbf{y} = \mathbf{0}$. \square

Using Eqn. 18 and Lemma 4 we have:

$$\frac{\|(\mathbf{L} + \Psi)\mathbf{x}\|_2}{\|\mathbf{x}\|_2} = \frac{\|\Psi\mathbf{x}\|_2}{\|\mathbf{x}\|_2} \leq \|\Psi\|_2 = \sigma_{\max}(\Psi), \quad (21)$$

where $\sigma_{\max}(\Psi)$ is the maximum singular value of Ψ .

Lemma 5. *Let $\mathbf{L} + \Psi \in \mathbb{R}^{N \times N}$ be full rank, then:*

$$\inf_{\mathbf{x} \neq \mathbf{0}} \frac{\|(\mathbf{L} + \Psi)\mathbf{x}\|_2}{\|\mathbf{x}\|_2} = \sigma_{\min}(\mathbf{L} + \Psi), \quad (22)$$

where $\sigma_{\min}(\mathbf{L} + \Psi)$ is the minimum singular value of $\mathbf{L} + \Psi$

Proof. Using the singular value decomposition $\mathbf{L} + \Psi = \tilde{\mathbf{U}}\Sigma\mathbf{V}^T$, and the fact that $\tilde{\mathbf{U}}$ and \mathbf{V} are unitary matrices we have:

$$\begin{aligned} \inf_{\mathbf{x} \neq \mathbf{0}} \frac{\|(\mathbf{L} + \Psi)\mathbf{x}\|_2}{\|\mathbf{x}\|_2} &= \inf_{\mathbf{x} \neq \mathbf{0}} \frac{\|\tilde{\mathbf{U}}\Sigma\mathbf{V}^T\mathbf{x}\|_2}{\|\mathbf{x}\|_2} = \inf_{\mathbf{x} \neq \mathbf{0}} \frac{\|\Sigma\mathbf{V}^T\mathbf{x}\|_2}{\|\mathbf{x}\|_2} \\ &\rightarrow \inf_{\mathbf{x} \neq \mathbf{0}} \frac{\|\Sigma\mathbf{V}^T\mathbf{x}\|_2}{\|\mathbf{x}\|_2} = \inf_{\mathbf{y} \neq \mathbf{0}} \frac{\|\Sigma\mathbf{y}\|_2}{\|\mathbf{V}\mathbf{y}\|_2} = \inf_{\mathbf{y} \neq \mathbf{0}} \frac{\|\Sigma\mathbf{y}\|_2}{\|\mathbf{y}\|_2} \\ &\rightarrow \inf_{\mathbf{y} \neq \mathbf{0}} \frac{\|\Sigma\mathbf{y}\|_2}{\|\mathbf{y}\|_2} = \inf_{\mathbf{y} \neq \mathbf{0}} \frac{(\sum_i |\sigma_i y_i|^2)^{\frac{1}{2}}}{(\sum_i |y_i|^2)^{\frac{1}{2}}}, \end{aligned}$$

where we used the change of variable $\mathbf{y} = \mathbf{V}^T\mathbf{x}$, and σ_i is the i -th singular value of $\mathbf{L} + \Psi$. Finally,

$$\begin{aligned} \frac{(\sum_i |\sigma_i y_i|^2)^{\frac{1}{2}}}{(\sum_i |y_i|^2)^{\frac{1}{2}}} &\geq \sigma_{\min}(\mathbf{L} + \Psi) \\ \rightarrow \inf_{\mathbf{x} \neq \mathbf{0}} \frac{\|(\mathbf{L} + \Psi)\mathbf{x}\|_2}{\|\mathbf{x}\|_2} &= \sigma_{\min}(\mathbf{L} + \Psi), \end{aligned}$$

where $\sigma_{\min}(\mathbf{L} + \Psi) = \sigma_N(\mathbf{L} + \Psi)$. \square

Using Eqn. 21, and lemma 5 we have:

$$\begin{aligned} \sigma_{\min}(\mathbf{L} + \Psi) &\leq \frac{\|(\mathbf{L} + \Psi)\mathbf{x}\|_2}{\|\mathbf{x}\|_2} \leq \sigma_{\max}(\Psi) \\ &\rightarrow \sigma_{\min}(\mathbf{L} + \Psi) \leq \sigma_{\max}(\Psi) \\ 1 &\leq \frac{\sigma_{\max}(\Psi)}{\sigma_{\min}(\mathbf{L} + \Psi)} \\ \sigma_{\max}(\mathbf{L} + \Psi) &\leq \sigma_{\max}(\Psi)\kappa(\mathbf{L} + \Psi) \\ \frac{\sigma_{\max}(\mathbf{L} + \Psi)}{\sigma_{\max}(\Psi)} &\leq \kappa(\mathbf{L} + \Psi), \end{aligned} \quad (23)$$

where $\kappa(\mathbf{L} + \mathbf{\Psi}) = \sigma_{\max}(\mathbf{L} + \mathbf{\Psi})/\sigma_{\min}(\mathbf{L} + \mathbf{\Psi})$ is the condition number in the ℓ_2 -norm of $\mathbf{L} + \mathbf{\Psi}$.

Now, using the triangle inequality of matrix norms

$$\begin{aligned} \|\mathbf{L} + \mathbf{\Psi}\|_2 &\leq \|\mathbf{L}\|_2 + \|\mathbf{\Psi}\|_2 \\ \rightarrow \sigma_{\max}(\mathbf{L} + \mathbf{\Psi}) &\leq \sigma_{\max}(\mathbf{L}) + \sigma_{\max}(\mathbf{\Psi}) \\ \kappa(\mathbf{L} + \mathbf{\Psi}) &\leq \frac{\sigma_{\max}(\mathbf{L}) + \sigma_{\max}(\mathbf{\Psi})}{\sigma_{\min}(\mathbf{L} + \mathbf{\Psi})}. \end{aligned} \quad (24)$$

Finally, using Eqn. 23 and 24 we have:

$$\frac{\sigma_{\max}(\mathbf{L} + \mathbf{\Psi})}{\sigma_{\max}(\mathbf{\Psi})} \leq \kappa(\mathbf{L} + \mathbf{\Psi}) \leq \frac{\sigma_{\max}(\mathbf{L}) + \sigma_{\max}(\mathbf{\Psi})}{\sigma_{\min}(\mathbf{L} + \mathbf{\Psi})}. \quad (25)$$

□

References

- [1] A. Anis, A. El Gamal, A. S. Avestimehr, and A. Ortega. A sampling theory perspective of graph-based semi-supervised learning. *IEEE Transactions on Information Theory*, 65(4):2322–2342, 2018. 2, 9
- [2] A. Anis, A. Gadde, and A. Ortega. Efficient sampling set selection for bandlimited graph signals using graph spectral proxies. *IEEE Transactions on Signal Processing*, 64(14):3775–3789, 2016. 1
- [3] M. Babae, D. T. Dinh, and G. Rigoll. A deep convolutional neural network for video sequence background subtraction. *Pattern Recognition*, 76:635–649, 2018. 6, 8
- [4] S. Bianco, G. Ciocca, and R. Schettini. Combination of video change detection algorithms by genetic programming. *IEEE Transactions on Evolutionary Computation*, 21(6):914–928, 2017. 6
- [5] T. Bouwmans. Traditional and recent approaches in background modeling for foreground detection: An overview. *Computer science review*, 11:31–66, 2014. 1, 2
- [6] T. Bouwmans, F. El Baf, and B. Vachon. Background modeling using mixture of Gaussians for foreground detection—a survey. *Recent Patents on Computer Science*, 1(3):219–237, 2008. 2
- [7] T. Bouwmans and B. Garcia-Garcia. Background subtraction in real applications: Challenges, current models and future directions. *arXiv preprint arXiv:1901.03577*, 2019. 1
- [8] T. Bouwmans, S. Javed, M. Sultana, and S. K. Jung. Deep neural network concepts for background subtraction: A systematic review and comparative evaluation. *Neural Networks*, 2019. 2
- [9] T. Bouwmans, A. Sobral, S. Javed, S. K. Jung, and E. H. Zahzah. Decomposition into low-rank plus additive matrices for background/foreground separation: A review for a comparative evaluation with a large-scale dataset. *Computer Science Review*, 23:1–71, 2017. 1
- [10] T. Bouwmans and E. H. Zahzah. Robust PCA via principal component pursuit: A review for a comparative evaluation in video surveillance. *Computer Vision and Image Understanding*, 122:22–34, 2014. 2
- [11] M. Braham, S. Piérard, and M. Van Droogenbroeck. Semantic background subtraction. In *IEEE International Conference on Image Processing*, pages 4552–4556. IEEE, 2017. 2, 6
- [12] S. Chen, R. Varma, A. Sandryhaila, and J. Kovačević. Discrete signal processing on graphs: Sampling theory. *IEEE Transactions on Signal Processing*, 63(24):6510–6523, 2015. 1, 3
- [13] S. Choo, W. Seo, D. Jeong, and N. I. Cho. Multi-scale recurrent encoder-decoder network for dense temporal classification. In *International Conference on Pattern Recognition*, pages 103–108. IEEE, 2018. 1
- [14] A. Gadde, A. Anis, and A. Ortega. Active semi-supervised learning using sampling theory for graph signals. In *ACM SIGKDD International Conference on Knowledge Discovery and Data Mining*, pages 492–501. ACM, 2014. 1
- [15] N. Goyette, P. M. Jodoin, F. Porikli, J. Konrad, and P. Ishwar. Changedetection.net: A new change detection benchmark dataset. In *IEEE Conference on Computer Vision and Pattern Recognition Workshops*, pages 1–8. IEEE, 2012. 1, 5
- [16] K. He, G. Gkioxari, P. Dollár, and R. Girshick. Mask R-CNN. In *IEEE International Conference on Computer Vision*, pages 2961–2969, 2017. 1, 3
- [17] K. He, X. Zhang, S. Ren, and J. Sun. Deep residual learning for image recognition. In *IEEE Conference on Computer Vision and Pattern Recognition*, pages 770–778, 2016. 3
- [18] S. Javed, A. Mahmood, T. Bouwmans, and S. K. Jung. Background-foreground modeling based on spatiotemporal sparse subspace clustering. *IEEE Transactions on Image Processing*, 26(12):5840–5854, 2017. 4
- [19] B. Jiang, Z. Zhang, D. Lin, J. Tang, and B. Luo. Semi-supervised learning with graph learning-convolutional networks. In *IEEE Conference on Computer Vision and Pattern Recognition*, pages 11313–11320, 2019. 9
- [20] V. Kalofolias. How to learn a graph from smooth signals. In *Artificial Intelligence and Statistics*, pages 920–929, 2016. 9
- [21] L. A. Lim and H. Y. Keles. Foreground segmentation using convolutional neural networks for multiscale feature encoding. *Pattern Recognition Letters*, 112:256–262, 2018. 1
- [22] T. Y. Lin, P. Dollár, R. Girshick, K. He, B. Hariharan, and S. Belongie. Feature pyramid networks for object detection. In *IEEE Conference on Computer Vision and Pattern Recognition*, pages 2117–2125, 2017. 1, 3
- [23] T. Y. Lin, M. Maire, S. Belongie, J. Hays, P. Perona, D. Ramanan, P. Dollár, and C. L. Zitnick. Microsoft COCO: Common objects in context. In *European Conference on Computer Vision*, pages 740–755. Springer, 2014. 2, 3
- [24] B. D. Lucas, T. Kanade, et al. An iterative image registration technique with an application to stereo vision. 1981. 4
- [25] L. Maddalena and A. Petrosino. The SOBS algorithm: What are the limits? In *IEEE Conference on Computer Vision and Pattern Recognition Workshops*, pages 21–26. IEEE, 2012. 6, 8
- [26] L. Maddalena and A. Petrosino. Towards benchmarking scene background initialization. In *International Conference on Image Analysis and Processing*, pages 469–476. Springer, 2015. 5

- [27] A. G. Marques, S. Segarra, G. Leus, and A. Ribeiro. Sampling of graph signals with successive local aggregations. *IEEE Transactions on Signal Processing*, 64(7):1832–1843, 2015. 1
- [28] T. Ojala, M. Pietikäinen, and T. Mäenpää. Multiresolution gray-scale and rotation invariant texture classification with local binary patterns. *IEEE Transactions on Pattern Analysis & Machine Intelligence*, (7):971–987, 2002. 4
- [29] A. Ortega, P. Frossard, J. Kovačević, J. M. F. Moura, and P. Vandergheynst. Graph signal processing: Overview, challenges, and applications. *Proceedings of the IEEE*, 106(5):808–828, 2018. 1
- [30] A. Parada-Mayorga, D. L. Lau, J. H. Giraldo, and G. R. Arce. Blue-noise sampling on graphs. *IEEE Transactions on Signal and Information Processing over Networks*, 5(3):554–569, 2019. 1
- [31] N. Perraudin, J. Paratte, D. Shuman, L. Martin, V. Kalofolias, P. Vandergheynst, and D. K. Hammond. GSPBOX: A toolbox for signal processing on graphs. *ArXiv e-prints*, Aug. 2014. 5, 6
- [32] I. Pesenson. Sampling in Paley-Wiener spaces on combinatorial graphs. *Transactions of the American Mathematical Society*, 360(10):5603–5627, 2008. 3
- [33] I. Pesenson. Variational splines and Paley-Wiener spaces on combinatorial graphs. *Constructive Approximation*, 29(1):1–21, 2009. 2, 4
- [34] M. Piccardi. Background subtraction techniques: A review. In *IEEE International Conference on Systems, Man and Cybernetics*, volume 4, pages 3099–3104. IEEE, 2004. 3, 4
- [35] D. Romero, M. Ma, and G. B. Giannakis. Kernel-based reconstruction of graph signals. *IEEE Transactions on Signal Processing*, 65(3):764–778, 2016. 1
- [36] A. Sandryhaila and J. M. F. Moura. Discrete signal processing on graphs. *IEEE Transactions on Signal Processing*, 61(7):1644–1656, 2013. 1
- [37] A. Sandryhaila and J. M. F. Moura. Big data analysis with signal processing on graphs: Representation and processing of massive data sets with irregular structure. *IEEE Signal Processing Magazine*, 31(5):80–90, 2014. 1
- [38] S. Shalev-Shwartz and S. Ben-David. *Understanding machine learning: From theory to algorithms*. Cambridge university press, 2014. 1
- [39] D. I. Shuman, S. K. Narang, P. Frossard, A. Ortega, and P. Vandergheynst. The emerging field of signal processing on graphs: Extending high-dimensional data analysis to networks and other irregular domains. *IEEE Signal Processing Magazine*, 30(3):83–98, 2013. 1
- [40] A. Sobral. BGSLibrary: An OpenCV C++ background subtraction library. In *IX Workshop de Viso Computacional*, 2013. 6
- [41] P. L. St-Charles, G. A. Bilodeau, and R. Bergevin. SuB-SENSE: A universal change detection method with local adaptive sensitivity. *IEEE Transactions on Image Processing*, 24(1):359–373, 2014. 6, 7, 8
- [42] P. L. St-Charles, G. A. Bilodeau, and R. Bergevin. A self-adjusting approach to change detection based on background word consensus. In *IEEE Winter Conference on Applications of Computer Vision*, pages 990–997. IEEE, 2015. 6, 7, 8
- [43] C. Stauffer and W. E. L. Grimson. Adaptive background mixture models for real-time tracking. In *IEEE Conference on Computer Vision and Pattern Recognition*, volume 2, pages 246–252. IEEE, 1999. 6, 8
- [44] M. O. Tezcan, J. Konrad, and P. Ishwar. A fully-convolutional neural network for background subtraction of unseen videos. *arXiv preprint arXiv:1907.11371*, 2019. 1
- [45] M. Tsitsvero, S. Barbarossa, and P. Di Lorenzo. Signals on graphs: Uncertainty principle and sampling. *IEEE Transactions on Signal Processing*, 64(18):4845–4860, 2016. 1
- [46] V. Vapnik. *The nature of statistical learning theory*. Springer science & business media, 2013. 1
- [47] K. Wang, Y. Liu, C. Gou, and F. Y. Wang. A multi-view learning approach to foreground detection for traffic surveillance applications. *IEEE Transactions on Vehicular Technology*, 65(6):4144–4158, 2015. 1
- [48] Y. Wang, Z. Luo, and P. M. Jodoin. Interactive deep learning method for segmenting moving objects. *Pattern Recognition Letters*, 96:66–75, 2017. 6
- [49] H. Weyl. Das asymptotische Verteilungsgesetz der Eigenwerte linearer partieller Differentialgleichungen (mit einer Anwendung auf die Theorie der Hohlraumstrahlung). *Mathematische Annalen*, 71(4):441–479, 1912. 5
- [50] Y. Wu, A. Kirillov, F. Massa, W. Y. Lo, and R. Girshick. Detectron2. <https://github.com/facebookresearch/detectron2>, 2019. 6
- [51] Z. Xu, B. Min, and R. C. C. Cheung. A robust background initialization algorithm with superpixel motion detection. *Signal Processing: Image Communication*, 71:1–12, 2019. 4
- [52] D. Zeng, X. Chen, M. Zhu, M. Goesele, and A. Kuijper. Background subtraction with real-time semantic segmentation. *IEEE Access*, 2019. 2
- [53] H. Zhao, J. Shi, X. Qi, X. Wang, and J. Jia. Pyramid scene parsing network. In *IEEE Conference on Computer Vision and Pattern Recognition*, pages 2881–2890, 2017. 2
- [54] W. Zheng, K. Wang, and F. Y. Wang. A novel background subtraction algorithm based on parallel vision and bayesian GANs. *Neurocomputing*, 2019. 2, 6, 7, 8